# Involvement of the Sieve Element Cytoskeleton in Electrical Responses to Cold Shocks[1][W]

**Jens B. Hafke*, Katrin Ehlers, Jens Föller, Sabina-Roxana Höll, Stefanie Becker, and Aart J.E. van Bel**

Plant Cell Physiology Group, Institute of Plant Physiology (J.B.H., S.-R.H., S.B.), and Plant Cell Biology Research Group, Institute of General Botany (J.B.H., K.E., J.F., S.B., A.J.E.v.B.), Justus-Liebig-University, D–35390 Giessen, Germany; and Institute of Botany, Justus-Liebig-University, D–35392 Giessen, Germany (K.E., J.F.)

This study dealt with the visualization of the sieve element (SE) cytoskeleton and its involvement in electrical responses to local cold shocks, exemplifying the role of the cytoskeleton in $Ca^{2+}$-triggered signal cascades in SEs. High-affinity fluorescent phalloidin as well as immunocytochemistry using anti-actin antibodies demonstrated a fully developed parietal actin meshwork in SEs. The involvement of the cytoskeleton in electrical responses and forisome conformation changes as indicators of $Ca^{2+}$ influx was investigated by the application of cold shocks in the presence of diverse actin disruptors (latrunculin A and cytochalasin D). Under control conditions, cold shocks elicited a graded initial voltage transient, $\Delta V_1$, reduced by external $La^{3+}$ in keeping with the involvement of $Ca^{2+}$ channels, and a second voltage transient, $\Delta V_2$. Cytochalasin D had no effect on $\Delta V_1$, while $\Delta V_1$ was significantly reduced with 500 nM latrunculin A. Forisome dispersion was triggered by cold shocks of 4°C or greater, which was indicative of an all-or-none behavior. Forisome dispersion was suppressed by incubation with latrunculin A. In conclusion, the cytoskeleton controls cold shock-induced $Ca^{2+}$ influx into SEs, leading to forisome dispersion and sieve plate occlusion in fava bean (*Vicia faba*).

It has been argued for a long time that sieve elements (SEs) are devoid of a cytoskeleton (Parthasarathy and Pesacreta, 1980; Thorsch and Esau, 1981; Evert, 1990), but more recent biochemical and cytological studies favor the opposite view. Actin as well as profilin were detected in phloem exudates of various monocot and dicot species (Schobert et al., 1998, 2000), while immunocytochemical tests showed the presence of actin and tubulin in phloem exudates of pumpkin (*Cucurbita maxima*; Kulikova and Puryaseva, 2002). Proteome analyses gave further credence to the occurrence of microfilaments in SEs in castor bean (*Ricinus communis*; profilin; Barnes et al., 2004), pumpkin (actin; Walz et al., 2004), canola (*Brassica napus*; actin, profilin1 and profilin2, actin-depolymerizing factor4; Giavalisco et al., 2006), and rice (*Oryza sativa*; actin1, actin-depolymerizing factor2, actin depolymerizing-factor3, and actin-depolymerizing factor6; Aki et al., 2008). Moreover, cytological evidence suggests residues of a cytoskeleton in SEs; fluorescent immunolabeling identified an actin/myosin system at the sieve plates (Chaffey and Barlow, 2002).

Theoretical considerations also call for the presence of a cytoskeleton in SEs. Turnover and addressing of macromolecules (Fisher et al., 1992; Leineweber et al., 2000) requires a local distribution network in SEs. This function was attributed to an endoplasmic reticulum (ER) continuous to the ER strands running through pore plasmodesma units (Blackman et al., 1998) into the companion cells. Although such a mechanism is essentially conceivable, an interaction between the ER and cytoskeleton would provide a more conventional mode of intracellular distribution (Hepler et al., 1990; Boevink et al., 1998; Ueda et al., 2010; Yokota et al., 2011; Chen et al., 2012). Moreover, macromolecular trafficking through pore plasmodesma units (Lucas et al., 2001) was proposed to be executed by actin and myosin (Oparka, 2004), implying the presence of a cytoskeleton in SEs. Despite the massive circumstantial evidence, however, a complete cytoskeleton network and its spatial distribution in SEs have not been visually documented thus far.

The existence of an SE cytoskeleton would raise questions regarding its task(s) in this highly specialized cell type. In other plant cells, the cytoskeleton was proposed to be engaged, among others, in ion channel operation and intracellular signaling (Trewavas and Malho, 1997; Mazars et al., 1997, and refs. therein; Thuleau et al., 1998; Örvar et al., 2000; Sangwan et al., 2001; Drøbak et al., 2004; Davies and Stankovic, 2006), as in animal cells (Janmey, 1998; Lange and Gartzke, 2006). For instance, $K^+$ fluxes are regulated by actin dynamics (Hwang et al., 1997; Liu and Luan, 1998; Chérel, 2004), while $Ca^{2+}$ influx into the cytoplasm appears to be mediated by voltage-dependent $Ca^{2+}$-permeable

[1] This work was supported by the Deutsche Forschungsgemeinschaft in the framework of Schwerpunktprogramm 1108.

* Corresponding author; e-mail jens.hafke@bot1.bio.uni-giessen.de.

The author responsible for distribution of materials integral to the findings presented in this article in accordance with the policy described in the Instructions for Authors (www.plantphysiol.org) is: Jens B. Hafke (jens.hafke@bot1.bio.uni-giessen.de).

[W] The online version of this article contains Web-only data.

www.plantphysiol.org/cgi/doi/10.1104/pp.113.216218

  

channels associated with microtubules (Mazars et al., 1997; Thion et al., 1998) or by mechanosensitive channels possibly associated with microfilaments (Wang et al., 2004; Zhang et al., 2007).

Both types of $Ca^{2+}$-permeable channels probably reside in the SE plasma membrane (Knoblauch et al., 2001; Hafke et al., 2007, 2009; Furch et al., 2009), where they are likely involved in $Ca^{2+}$-dependent systemic signaling (Furch et al., 2009; Hafke et al., 2009; van Bel et al., 2011; Hafke and van Bel, 2013). These channels are also putative initiators of $Ca^{2+}$-induced signal transduction in SEs, leading to sieve-plate occlusion in response to local cold shocks (Thorpe et al., 2010). In fava bean (*Vicia faba*), $Ca^{2+}$-dependent sieve tube occlusion by dispersion of special phloem-specific proteins (P-proteins) known as forisomes has been studied intensely (Knoblauch et al., 2001; Furch et al., 2007, 2009; Thorpe et al., 2010). Thus, apart from its distributive tasks, a cytoskeleton may be of major importance for intracellular signaling cascades in the highly specialized, sparsely equipped SEs.

Our objective was to investigate the existence and spatial distribution of an SE cytoskeleton and its engagement in local signaling through $Ca^{2+}$ influx brought about by cold shocks. This study dealt with the visualization of cytoskeletal components in intact sieve tubes using microinjection of fluorescent phalloidin and immunocytochemistry. Confocal laser-scanning micrography (CLSM) and transmission electron microscopy unequivocally showed a parietally located cylindrical actin meshwork. We demonstrated the engagement of the network in local cold shock-induced electrical responses and its association with $Ca^{2+}$ influx, since we found effects of the $Ca^{2+}$ channel blocker $La^{3+}$ and of the cytoskeleton disruptor latrunculin A (LatA) on electrical signatures triggered by cold shocks and, by consequence, on forisome conformation changes.

## RESULTS

### Fluorescence-Labeled Phalloidin Binds to Actin in SEs of Fava Bean

Due to the extreme sensitivity of the SE substructure to invasive treatments, information on the spatial distribution of the actin meshwork in SEs is scarce (Chaffey and Barlow, 2002). Hence, the existence of a complete cytoskeleton in SEs is a matter of dispute to date. To acquire conclusive information on its existence and location, it is preferable to use noninvasive methods. However, phloem tissues are buried deep inside the plant body, which requires the removal of overlying tissues to enable physiological tests. Attempts to load the fluorescent actin probe phalloidin (fl-phal; Alexa Fluor 546) into tissues pretreated with fixatives or detergents (Lloyd, 1988; Tiwari and Polito, 1988; Heslop-Harrison and Heslop-Harrison, 1997) were not successful for fava bean sieve tubes. All in all, careful pressure-driven microinjection into living sieve tubes embedded in intact plants (Hafke et al., 2005) turned out to be the optimal compromise to visualize and characterize the cytoskeleton in fava bean SEs (Fig. 1). In addition, immunocytochemistry was applied to verify the existence of a cytoskeleton in SEs (Figs. 2 and 3).

Following the few successful microinjections ($n$ = 10), fluorescence due to fl-phal association with actin filaments (Fig. 1) was observed by CLSM. High-affinity binding of phalloidin to actin filaments has often been demonstrated (Lengsfeld et al., 1974; Cooper, 1987). Because the impalement of microcapillaries into intact SEs triggered sieve plate occlusion (Knoblauch and van Bel, 1998), actin-associated fluorescence remained restricted to one SE. Since SEs were seldom in the plane of focus over their entire length, smaller regions along the SE were scanned, allowing a higher resolution of the microfilament network (Fig. 1, B–J).

Optical sections from four of the 10 successful microinjections are shown in Figure 1. The images show optical sections from the sieve plate region (Fig. 1, D–G and I) and the middle region of an SE (Fig. 1, B, C, H, and J), which includes the area around the forisome (Fig. 1, B, C, and H). The micrographs (Fig. 1A) reveal a continuous microfilament meshwork extending throughout the entire SE. In addition to CLSM scans in one focus plane (Fig. 1A), Z scans were performed after fl-phal injection to obtain a better resolution of the three-dimensional structure (Fig. 1, D–G). To this end, the top optical section (Fig. 1F), the middle section (Fig. 1, D and E), as well as the bottom section of an SE (Fig. 1G) were scanned. The top and bottom sections exhibited an area-wide actin meshwork, while the middle section showed actin filaments appressed to the plasma membrane. The images demonstrate collectively that actin forms a parietal cylinder-shaped meshwork located the SE mictoplasm.

We observed a highly fluorescent envelope around the forisome (Fig. 1, A and B), possibly an unspecific staining, as found for the binding of other fluorochromes to forisomes (Knoblauch and van Bel, 1998). Microfilaments aggregated in the region around the penetration site (Fig. 1, A, H, and J), possibly due to the local wounding effects. A massive fl-phal labeling was detected in the sieve plate region (Fig. 1, A and I).

To exclude unspecific binding of the fluorochrome group (Alexa Fluor 546) of fl-phal to diverse filamentous structures and to confirm the specific binding of fl-phal to actin filaments, we microinjected a reactive Alexa Fluor 546 derivative, *N*-hydroxysuccinimidylester (NHS-ester), into SEs, which is known to bind to amino groups of proteins (Fig. 1, K and L). Forisome staining and other protein clogs in the SE lumen as well as weakly fluorescent spots in the mictoplasm region (Fig. 1K) were visible, but a filamentous network as observed with fl-phal injections was not detectable. Hydrolyzing the NHS-ester group in alkaline medium leads to loss of its protein-binding properties. Microinjection of the

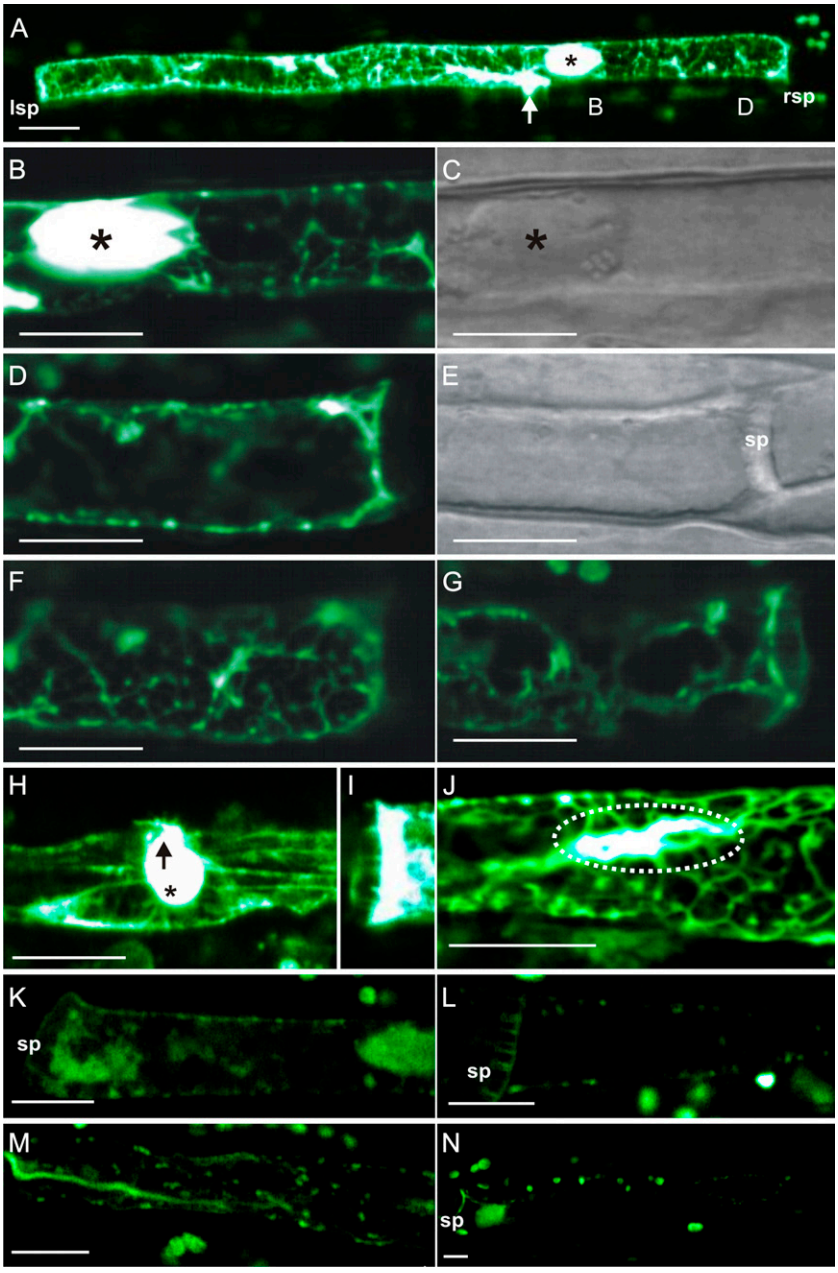


**Figure 1.** The fl-phal distribution after pressure-driven microinjection in SEs of fava bean. A, Fluorescence arising from microinjected fl-phal bound to actin filaments was detected by observing intact sieve tubes using CLSM. The site of injection (arrow) and the dispersed forisome (asterisk) are marked. lsp, Left sieve plate; rsp, right sieve plate. B to G, Longitudinal sections along an SE scanned to reach a higher resolution of the microfilament arrangement. B, From left to right: magnification of region B as marked in A in which the forisome (asterisk) is located. A strong staining by fl-phal is visible around the forisome (asterisk) and the microcapillary penetration site. C, Light-transmission version of B. D to G, Longitudinal Z scans of the right sieve plate region D as marked in A including a middle section (D) with the light-transmission version (E), an upper SE section (F), and a lower section (G). H, Typical aggregation of microfilaments around the microelectrode penetration site (arrow) in the vicinity of a dispersed forisome (asterisk) in another SE. I, Microfilament staining at the sieve plate region of a third SE. J, Visualization of the parietal actin network in another SE following fl-phal injection. Note the accumulation of fluorescence (dotted oval) around the microcapillary penetration site as in A and H. K and L, Control staining by microinjection of a highly reactive Alexa Fluor 546 NHS-ester derivative into SEs of fava bean. NHS-esters are known to bind to primary amino groups of biomolecules. sp, Sieve plate. M and N, Control staining by microinjection of the hydrolyzed inactive Alexa Fluor 546 NHS-ester derivative into SEs of fava bean. Hydrolysis causes the loss of its binding properties. Bars = 10 $\mu$m.

hydrolysate into SE ($n$ = 3) resulted in a diffuse staining within the SEs (Fig. 1, M and N). All in all, these experiments indicate that the active agent binding to the parietal filaments in SEs is phalloidin rather than the fluorochrome group Alexa Fluor 546.

### Immunocytochemical Visualization of a Parietal Actin Network in SEs

As an independent approach, immunocytochemistry was used to test the presence of a mictoplasmic cytoskeleton at higher resolution (Fig. 2) and to demonstrate that fl-phal binding to forisomes was unspecific (Fig. 1, B and H). Ultrathin phloem sections were labeled with clone C4 anti-actin antibody using two different dilutions and stringent or less stringent washing conditions (Figs. 2, A–D, and 3). Controls were incubated with buffer alone (Fig. 2E), and all sections were treated with 5-nm gold-labeled secondary antibodies. The anti-actin antibody labeled a fine-meshed parietal network in the SE mictoplasm, consisting of filamentous structures with low electron density located at the periphery of SEs in the vicinity of the plasma membrane (Fig. 2, A–D). No significant label occurred in the SE lumina (Fig. 2, C and D), at the SE cell walls (Figs. 2, A and D, and 3C), or at the callose collars surrounding the sieve pores (Fig. 3, C and

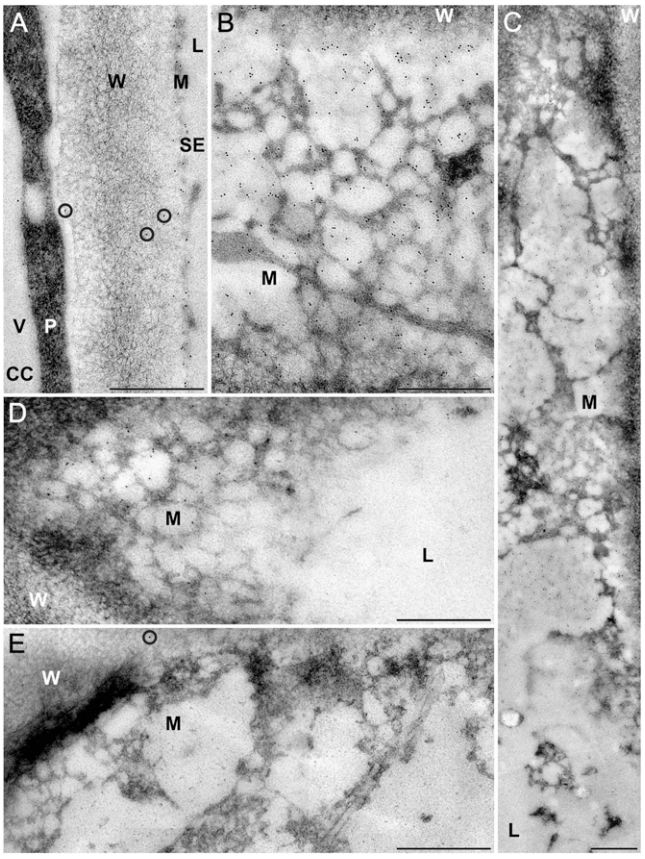


**Figure 2.** Immunocytochemical visualization of a parietal actin network in SEs of fava bean. For indirect immunolocalization, ultrathin sections were labeled with clone C4 anti-actin (dilution in A–C, 1:100; dilution in D, 1:200) or with buffer (control; E) and treated with 5-nm gold-labeled secondary antibodies. Washing conditions were less stringent in A to C than in D and E. Antibodies label a fine-meshed network with a low electron density located at the periphery of the SEs close to the plasma membrane (A–D). In SEs longitudinally sectioned in a median plane (A), the network is cross sectioned and, therefore, barely visible. In oblique sections through the longitudinal axis of an SE (B–D) passing through the central SE lumen (L), the mictoplasm (M), and the wall (W), the densely labeled parietal network is clearly visible in top view. No label occurs in the central lumen of the SEs (C and D) and in the vacuoles (V) of adjacent companion cells (CC in A) and phloem parenchyma cells. The cytoplasm (P) of the adjacent cells is regularly, but not densely, labeled (A). Labeling of the parietal SE network is particularly strong on sections treated with a high concentration of primary antibody (dilution, 1:100) and less stringent washing conditions (A–C). Here, some nonspecific labeling occurs on the cell walls of the SEs (circles in A). This background labeling was eliminated by using a lower concentration of primary antibody (dilution, 1:200) and more stringent washing conditions (D). With this procedure, labeling of the parietal SE network is slightly reduced but still prominent (D). It differs significantly from that of control sections, which were treated with secondary antibody only and show a negligible amount of nonspecific labeling (circle in E). Bars = 500 nm.

D). The labeling pattern is in a good agreement with the results obtained by microinjection of fl-phal into SEs (Fig. 1). The absence of forisome labeling in the condensed (Fig. 3A) and dispersed (Fig. 3B) states corroborated our above assumption that forisome staining by fl-phal is due to unspecific binding (Fig. 1). Furthermore, the high resolution obtained by antibody labeling revealed that the parietal actin network actually continued through the peripheral mictoplasma layer covering the sieve pores (Fig. 3D), which is in line with the finding that fl-phal binds at the sieve plates (Fig. 1, A and I).

### Involvement of the SE Cytoskeleton in Local Electrical Responses to Cold Shocks

In cell types other than SEs, the cytoskeleton is involved in the response to local environmental stimuli such as cold shocks (Mazars et al., 1997). Here, we investigated the impact of cytoskeleton disruptors on voltage transients following local cold shocks in SEs, which are associated with $Ca^{2+}$-dependent sieve plate occlusion by forisome dispersion (Thorpe et al., 2010). Electrical responses to cold shocks were recorded using microelectrodes impaled into SEs (Fig. 4, A and B) in intact phloem tissues submersed in bathing medium. Identical experiments were carried out with SEs preincubated with the membrane-impermeant $Ca^{2+}$ channel blocker $La^{3+}$ (Hille, 1992) or with the membrane-permeant cytoskeleton disruptors LatA and cytochalasin D (CytD), which degrade actin filaments (Cooper, 1987; Spector et al., 1989).

### Electrical Responses to Local Cold Shocks under Control Conditions and after Treatment with the Membrane-Impermeant $Ca^{2+}$ Channel Blocker $La^{3+}$

After stabilization of the membrane potential ($V_m$) subsequent to microelectrode insertion into SEs, cold shocks were applied to the impaled SEs, and changes in $V_m$ were recorded. Cold shocks, defined as very rapid but brief cooling (Thorpe et al., 2010), were expressed as temperature drops ($\Delta T$; i.e. the differences between the initial temperature before the cold shock and the lowest temperature reached during the cold shock). $\Delta T$ varied between 1.5°C and 16°C starting from ambient temperatures between 22°C and 27°C (Fig. 4, C and E).

Cold shocks elicited voltage transients (also referred to as "signals" here and in the figures) with variable shapes in SEs of control plants, as demonstrated previously (Minorsky and Spanswick, 1989; Thorpe et al., 2010). These transients were often biphasic. The initial transient (first peak, $\Delta V_1$), used as the first parameter to characterize the electrical signature, either repolarized quickly and almost reached the $V_m$ resting level (Fig. 4C, first signal) or passed into a plateau phase (Fig. 4C, second signal), or it was followed by a second smaller depolarization ($\Delta V_2$; Fig. 4C, third signal) before the $V_m$ resting level was restored. As the second parameter to characterize the electrical signature, we defined $\Delta V_2$ as the voltage difference between plateau phase or further maximum depolarization (second peak)

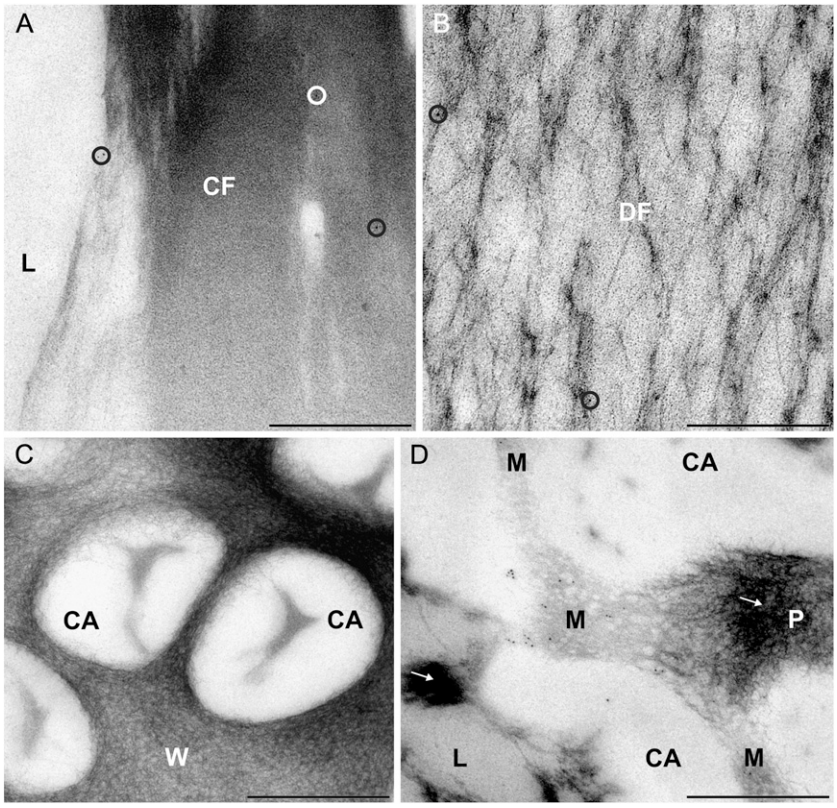


**Figure 3.** Immunoreactivity of forisomes and sieve pores of fava bean SEs to actin antibodies. For indirect immunolocalization, ultrathin sections were labeled with clone C4 anti-actin (dilution, 1:200) and 5-nm gold-labeled secondary antibodies. Washing conditions were stringent. Nonspecific labeling is reduced to a negligible amount (circles in A and B) on condensed forisomes (CF in A) and dispersed forisomes (DF in B) lying in the lumen (L) of the SEs. No label occurs on the cell wall areas of the sieve plates (W in C) and on the callose collars surrounding the sieve pores (CA in C and D). A significant labeling is visible in an oblique section through a sieve pore (D), passing through the SE lumen (L) with aggregated P-proteins (arrow), the callose collar (CA), the plasma membrane and the mictoplasm (M), and the sieve pore lumen (P) plugged with P-proteins (arrow). The labeling occurs in the tangentially sectioned mictoplasm close to the plasma membrane and probably marks junctions of the parietal actin network in SEs passing through the sieve pores. Labeling is insignificant on aggregated P-proteins (arrows in D). Bars = 500 nm.

and the $V_m$ resting level. The sizes of $\Delta V_1$ and $\Delta V_2$ appeared to be $\Delta T$ dependent (Fig. 4, C, E, and F). As demonstrated in Figure 4C (see also Fig. 4J), the duration of the repolarization showed a high variability that mainly relied on the duration of $\Delta V_2$ (Fig. 4G). A prominent $\Delta V_2$ phase of the electrical signature was only detected when $\Delta V_1$ had reached a threshold value of approximately 100 mV (Fig. 4H), which corresponds to the maximum value of $\Delta V_1$ (Fig. 4E). Both phases of the voltage transient were reduced by externally applied 1 mM $La^{3+}$, an inhibitor of $Ca^{2+}$-permeable channels (Fig. 4, D–F), which is consistent with the engagement of $Ca^{2+}$-permeable channels at the plasma membrane in cold responses as reported before (Minorsky and Spanswick, 1989; Knight et al., 1996; Lewis and Spalding, 1998; Plieth et al., 1999).

### Analysis of Voltage Transients and Forisome Responses Triggered by Local Cold Shocks

*Analysis of $\Delta V_1$*

A clear correlation between cold shock intensity and electrical response was also reported for cells of *Cucurbita* spp. seedlings (Minorsky and Spanswick, 1989). The amplitude of the first transient $\Delta V_1$ measured in SEs fitted best to the amplitude of the $\Delta T$ in a sigmoid fashion (Fig. 4E; $r^2 = 0.88$). Data points were fitted to a dose ($\Delta T$)-response ($\Delta V_1$) curve with variable slope (H, for Hill coefficient), as given by Equation 1:

$$\Delta V_1 = \Delta V_{1min} + \frac{\Delta V_{1max} - \Delta V_{1min}}{1 + 10^{(\Delta T(V_{0.5}) - \Delta T)H}} \quad (1)$$

Fitting procedures yielded a maximum ($\Delta V_{max}$) and minimum ($\Delta V_{min}$) depolarization of 102 and 31 mV, respectively, a $\Delta T$ at a half-maximum depolarization [$\Delta T$ ($V_{0.5}$)] of 3.23°C, and H of 1.14 ($r^2 = 0.88$). The maximum depolarization $\Delta V_1$ (approximately 100 mV) was reached at $\Delta T > 4$°C and did not increase with higher $\Delta T$ values. Linear plots of the same parameters showed lower correlation coefficients (data not shown). In the presence of 1 mM $La^{3+}$, the electrical response to $\Delta T$ showed a pronounced reduction of $\Delta V_1$ by approximately 50% as compared with control measurements (Fig. 4, D and E).

*Analysis of $\Delta V_2$*

$\Delta V_2$ increased with the strength of $\Delta T$, yielding almost identical correlation coefficients in linear fittings (data not shown; $r^2 = 0.81$) or sigmoidal fittings (Fig. 4F; Eq. 1 for $\Delta V_2$; $\Delta V_{2max} = 41.9$ mV, $\Delta V_{2min} = -3.3$ mV; H = 0.16; $r^2 = 0.84$). The slower kinetics of $\Delta V_2$ compared with the spike-like shape of $\Delta V_1$ was mirrored by a $\Delta T(V_{0.5})$ of 6°C. In contrast to $\Delta V_1$, $\Delta V_2$ was entirely suppressed by $La^{3+}$ in three of seven measurements (Fig. 4F). The amplitude of $\Delta V_2$ had a strong effect on the duration of the entire electrical signature, given the linear correlation between signal duration and $\Delta V_2$ (Fig. 4G; $r^2 = 0.81$).

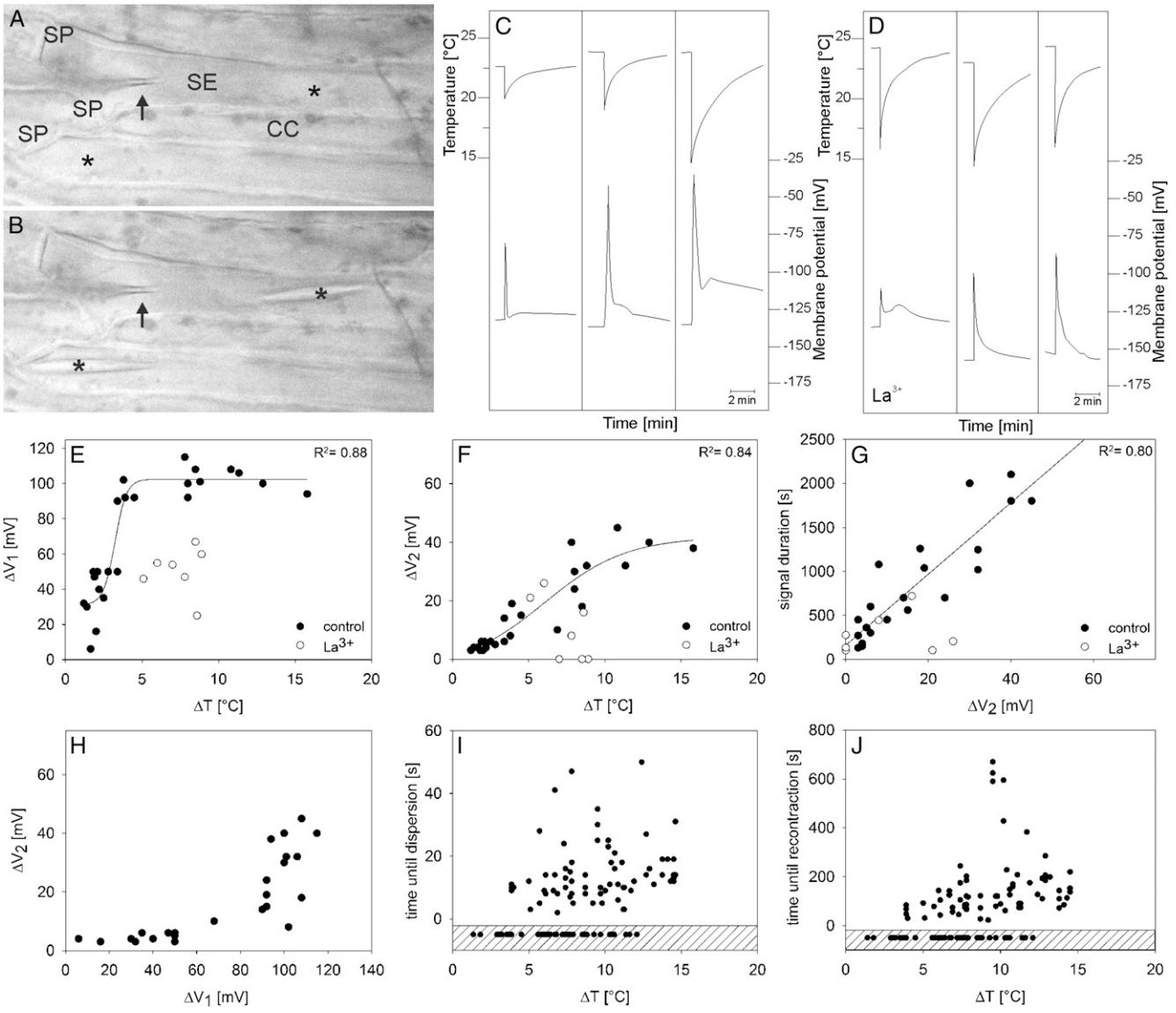


**Figure 4.** Effect of cold shocks (abrupt cooling and rewarming) on SE $V_m$. A, After microelectrode impalement into an SE, forisomes (asterisks) disperse in response to $Ca^{2+}$ influx triggered by the local wounding. cc, Companion cell; sp, sieve plate. B, Recondensed forisomes in recovered SEs that are ready for cold shocks. The microelectrode tip is indicated by the arrow. C, Three typical cold shock-triggered (top graphs) electrical responses (bottom graphs) recorded in different SEs under control conditions in BM. The time courses of cold shocks were recorded by a thermocouple, and electrical responses were recorded by voltage-sensitive microelectrodes. D, Three typical cold shock-triggered (top graphs) electrical responses (bottom graphs) recorded in different SEs preincubated with 1 mM $La^{3+}$. E, Relationship between cold shocks (expressed as ΔT, the difference between the initial temperature before the cold shock and the lowest temperature reached during the cold shock) and the peak of the first voltage transient ($\Delta V_1$) recorded in SEs under control conditions (black circles; $n = 25$) and after preincubation with 1 mM $La^{3+}$ (white circles; $n = 8$). Data points of the control curve were fitted to sigmoid correlation (according to Eq. 1). F, Relationship between the peak of the second voltage transient ($\Delta V_2$) and the cold shock (ΔT) under control conditions and preincubated in the membrane-impermeant 1 mM $La^{3+}$. Data points of the control curve were fitted to Equation 1. G, Relationship between the entire signal length and the peak of the second voltage transient ($\Delta V_2$) under control conditions and after preincubation of SEs with 1 mM $La^{3+}$. H, Correlation between the voltage transients $\Delta V_2$ and $\Delta V_1$ under control conditions. I and J, Correlation between forisome response time (time until dispersion; I) as well as recovery time (time until recontraction; J) and cold shocks (ΔT) under control conditions (Thorpe et al., 2010). The quantity of nonreactive forisomes is displayed in the dashed areas of I and J.

When $\Delta V_2$ was plotted against $\Delta V_1$ (Fig. 4H), $\Delta V_2$ remained lower than 10 mV until maximum $\Delta V_1$ (approximately 100 mV) was reached. Then, $\Delta V_2$ increased abruptly, showing a high variability.

### Forisome Responses

Forisome reaction was observed as an SE response to cold shocks (Thorpe et al., 2010). Since forisome dispersion in fava bean was shown to be $Ca^{2+}$ dependent (Knoblauch et al., 2001), forisomes were used as optical indicators for $Ca^{2+}$ influx during cold shocks (Thorpe et al., 2010). Forisome dispersion seemed to be temperature independent under the present experimental conditions from a threshold value of around $\Delta T = 4°C$ (Fig. 4I). Forisome dispersion and, hence, sufficient $Ca^{2+}$ influx (Hafke et al., 2009) takes place within 5 to 50 s after the cold shock (Fig. 4I). It became obvious that full forisome dispersion above a $\Delta T$ of 4°C (Fig. 4I) requires the maximum $\Delta V_1$ value of around 100 mV (Fig. 4E) and that forisome dispersion is related to $\Delta V_1$.

Analogous to the dispersion behavior, the recontraction time of forisomes showed no distinct temperature dependence above 4°C (Fig. 4J). The period for recontraction varied between 30 and 670 s. Similar time frames for forisome dispersion and recontraction were found for remote burning stimuli (Furch et al., 2009).

### Impact of the Membrane-Permeant Actin Disruptor LatA on the Electrical Profiles Triggered by Cold Shocks

As demonstrated above, microinjections of fl-phal (Fig. 1) and immunolocalization by transmission electron microscopy (Figs. 2 and 3) revealed the presence of a fully developed mictoplasmic actin meshwork. To test the hypothesis that the cytoskeleton controls $Ca^{2+}$ influx (and forisome dispersion) brought about by cold shocks, we investigated the impact of the microfilament disruptor LatA (Fig. 5A), of a mixture of LatA and $La^{3+}$ (Fig. 5B), and of CytD (Supplemental Fig. S1) on electrical signatures and forisome responses triggered by cold shocks. LatA, a membrane-permeant macrolide, is known to hinder microfilament polymerization due to a one-to-one binding with monomeric G-actin (Spector et al., 1989). In comparison with cell membrane-permeable CytD, LatA has a 10- to 100-fold greater potential for actin microfilament disruption and keeps treated cells in their altered state for several hours (Spector et al., 1989). In line with this, pretreatment of SEs with 500 nM LatA or 500 nM LatA and 1 mM $La^{3+}$ significantly reduced the amplitude of $\Delta V_1$ (Fig. 5, A and B) as compared with control measurements (Fig. 4C) or in SEs pretreated with 40 $\mu$M CytD (Supplemental Fig. S1A).

Dimethyl sulfoxide (DMSO) at the concentrations used here had no effect on electrical responses, as indicated by a barely reduced $\Delta V_1$ with 250 nM LatA at shorter (1–1.5 h) incubation times (Fig. 5C; Supplemental Fig. S1A). LatA at 500 nM, but not at 250 nM, had a significant effect on $\Delta V_1$ (Fig. 5C). The amplitude of the first transient ($\Delta V_1$) after pretreatment with 500 nM LatA fitted best to $\Delta T$ in a sigmoid fashion with a $\Delta T(V_{0.5})$ of 3.4°C (Eq. 1; $\Delta V_{max}$ = 66.4 mV, $\Delta V_{min}$ = 13.6 mV; H = 0.62; $r^2$ = 0.84; Fig. 5C), which matches the value found for control measurements [$T(V_{0.5})$ = 3.23°C; Fig. 4E]. The lower Hill coefficient (H = 0.62) as compared with control measurements (H = 1.14; Fig. 4E), as well as the lower $\Delta V_{min}$ and $\Delta V_{max}$, are indicative of a loss of temperature dependence of a putative temperature sensor in SEs due to LatA pretreatment.

Coincubation of 500 nM LatA and 1 mM $La^{3+}$ (Fig. 5D) reduces $\Delta V_1$ by only 10 to 20 mV as compared with LatA alone (Fig. 5C), reaching the magnitude obtained for pure $La^{3+}$ treatments (Fig. 4E), which suggests that $La^{3+}$ and LatA act on the same $Ca^{2+}$ influx system. In line with this, LatA (500 nM) and $La^{3+}$ pretreatments prevented any form of forisome dispersion in response to cold shocks over a temperature range of 3°C to 15°C ($n$ = 25). In contrast to the effect of LatA (500 nM) and $La^{3+}$, forisome dispersion takes place in CytD-pretreated tissues ($n$ = 20; Supplemental Fig. S1, B and C) above a threshold of $\Delta T$ = 4°C ($n$ = 20), as observed for control measurements (Fig. 4, I and J). Even more clear than after $La^{3+}$ treatment alone (Fig. 4F), complete suppression of $\Delta V_2$ was achieved in the presence of the mixture $La^{3+}$/LatA (500 nM; Fig. 5E) in 13 of 14 measurements, which caused a strong reduction of the repolarization period (Fig. 5F). This implies that LatA acts, directly or indirectly, on a second process associated with the $V_2$ phase. The value of $\Delta V_1$ to activate $\Delta V_2$ shifts from 100 mV (control; Fig. 4H) to about 60 mV in the presence of LatA (Fig. 5G), which corresponds to the maximum value of $\Delta V_1$ reached after pretreatment with 500 nM LatA (Fig. 5C).

## DISCUSSION

### SEs Contain a Peripheral Mictoplasmic Actin Meshwork

Microinjection of fl-phal (Fig. 1) and immunocytochemical localization (Figs. 2 and 3) showed that actin filaments form an evenly distributed, parietal cylindrical meshwork through the entire SE and crossing sieve plates (Fig. 3). Thus, the SE cytoskeleton is definitely more complete than the "acto-myosin systems" observed in the vicinity of the sieve plates (Chaffey and Barlow, 2002).

Aggregations of actin filaments around the penetrated electrode tip (Fig. 1, H and J) deviate clearly from the distribution in the rest of the SE. In animal cells, the formation of filament bundles at sites of mechanical stress ("stress fibers"; Janmey, 1998, and refs. therein) was postulated to activate mechanosensitive $Ca^{2+}$ channels (Hayakawa et al., 2008). Hence, mechanical stress exerted by the electrode tip may have led to the channel-mediated $Ca^{2+}$ influx responsible for forisome dispersion (Fig. 4A), supplementing the $Ca^{2+}$ influx from the apoplasm via the initial, but temporary, tip wound, as discussed before (Will and van Bel, 2006).

### Local Cold Shocks Trigger Graded Electrical Responses ($\Delta V_1$ and $\Delta V_2$) Associated with $Ca^{2+}$ Influx

Local cold shocks elicit electrical response profiles including two distinct kinetic components called $\Delta V_1$

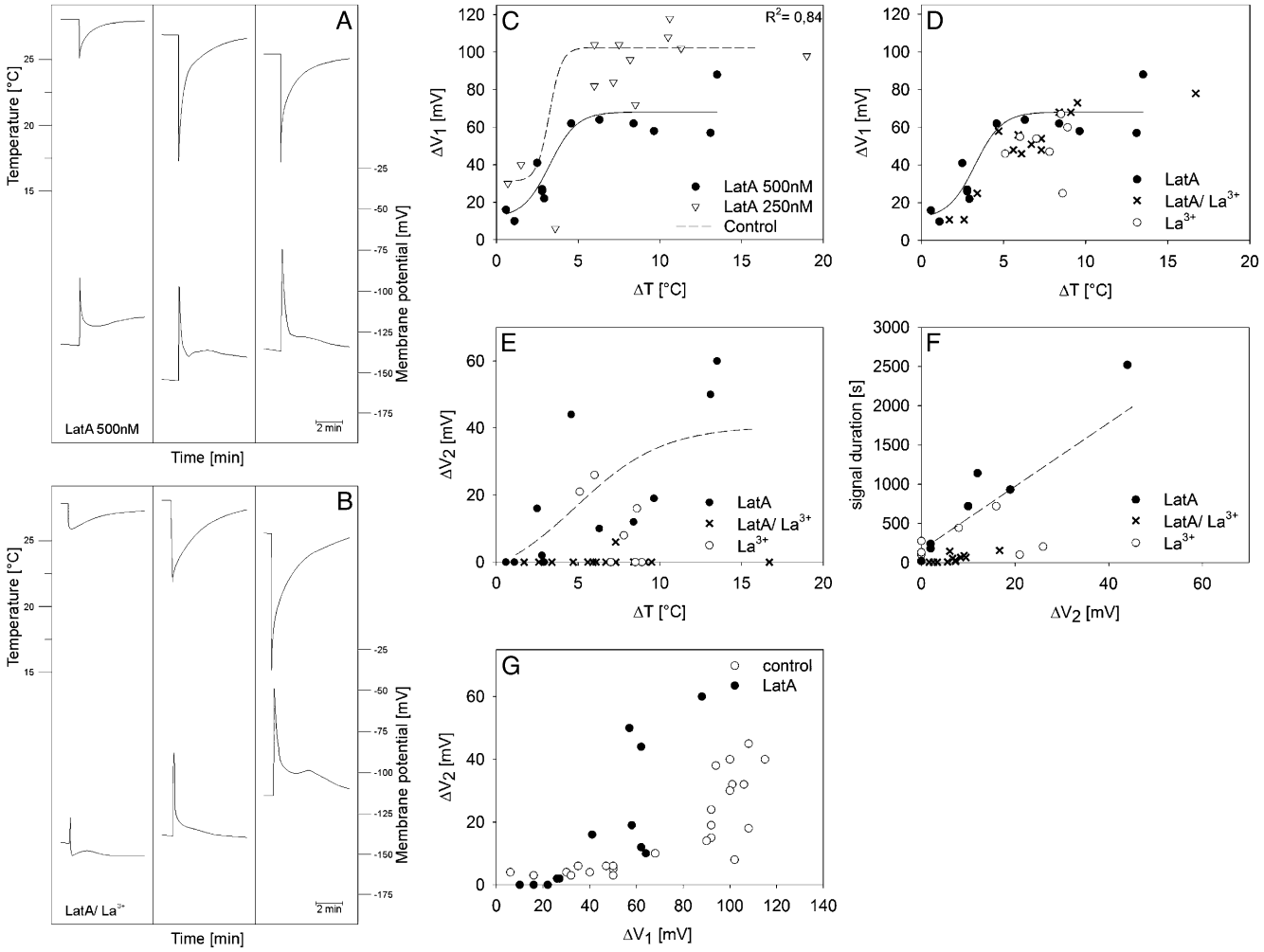


**Figure 5.** Effects of cold shocks on the $V_m$ of SEs pretreated with the membrane-permeant cytoskeleton disruptor LatA. A and B, Time courses of three typical electrical responses triggered by cold shocks (ΔT) recorded from SEs preincubated in 500 nM LatA for 2 h ($n$ = 12; A) or in a mixture of 500 nM LatA and 1 mM $La^{3+}$ for 2 h ($n$ = 14; B). The time courses of cold shocks (top graphs) were recorded by a thermocouple, and electrical responses (bottom graphs) were recorded by voltage-sensitive microelectrodes. C to E, Relationships between cold shocks, expressed as the ΔT applied to SEs pretreated with LatA (C, 250 nM, 1–1.5 h, and 500 nM, 2 h; D and E, 500 nM) and LatA/$La^{3+}$ (D, 500 nM/1 mM, 2 h) and $\Delta V_1$ (C and D) and $\Delta V_2$ (E). Data points for $La^{3+}$ in D and E were taken from Figure 4, E and F. F, Relationship between the entire signal length and the peak of the second voltage gradient ($\Delta V_2$) after cold shock observed with SEs pretreated with 500 nM LatA (black circles) and 500 nM LatA/1 mM $La^{3+}$ (crosses). $La^{3+}$ controls (white circles) were taken from Figure 4G. G, Correlation between voltage transients $\Delta V_2$ and $\Delta V_1$ for SEs preincubated in 500 nM LatA for 2 h. Control values (untreated SEs; white circles) were taken from Figure 4H.

and $\Delta V_2$ in SEs (Thorpe et al., 2010). The initial fast transient $\Delta V_1$ merges into a second slower depolarization or a plateau phase until the $V_m$ resting level is attained (Fig. 4C). The maximal amplitude of $\Delta V_1$ of about 100 mV was reached for cold shocks with ΔT of 4°C to 5°C and more (Fig. 4, C and E), which is in line with observations for parenchymatous cells of *Cucurbita* spp. (Minorsky and Spanswick, 1989) and Arabidopsis (*Arabidopsis thaliana*; Carpaneto et al., 2007). The amplitude of $\Delta V_1$ fits best to ΔT in a sigmoidal fashion, with a half-maximal depolarization at ΔT of 3.2°C (Fig. 4E). This value is in the range of ΔT under natural conditions like wind chill or dripping melt water.

Sharp voltage transients ($\Delta V_1$) elicited by local cold shocks have been linked to the action of $Ca^{2+}$-permeable channels localized at the plasma membrane (Minorsky and Spanswick, 1989; Ding and Pickard, 1993; Lewis et al., 1997; White, 2009, and refs. therein). In keeping with this concept, the cell-impermeant $Ca^{2+}$ channel blocker $La^{3+}$ decreased $\Delta V_1$ by about 50% (Fig. 4, D and E). Furthermore, forisome dispersion within 5 to 50 s after cold shock (Fig. 4I) indicates $Ca^{2+}$ influx during the electrical response, since the forisome response requires large local near-plasma membrane $Ca^{2+}$ gradients (Furch et al., 2009; Hafke et al., 2009). Forisome dispersion and $\Delta V_1$ are strictly correlated, as

shown by identical ΔT thresholds (approximately 4°C; Fig. 4I) for maximal $\Delta V_1$ (Fig. 4E) and forisome dispersion (Fig. 4I). The all-or-none threshold for forisome dispersion may reflect a critical initial $Ca^{2+}$ dose at which $Ca^{2+}$ release from internal stores is induced. $Ca^{2+}$ mobilization from stores such as the ER and vacuoles is an established reaction to cold responses (Knight et al., 1996; Krol et al., 2003, and refs. therein). This $Ca^{2+}$ recruitment from internal stores, possibly by $Ca^{2+}$-induced $Ca^{2+}$ release from smooth ER cisternae (Furch et al., 2009; Hafke et al., 2009), may be required for the dispersion of forisomes, the ends of which seem to be in touch with the smooth ER (Furch et al., 2009; Hafke and van Bel, 2013).

Local cold shocks less than 4°C (Fig. 4, C and E) resulted in fast, dose-dependent voltage transients characterized by the absence of a distinct $\Delta V_2$ (Fig. 4, C and I). Such dose-dependent voltage transients may be accompanied by a transient rise in $Ca^{2+}$ permeability (Krol and Trebacz, 1999; Krol et al., 2003, 2004) but may not recruit sufficient $Ca^{2+}$ from internal stores to trigger a forisome response (Hafke et al., 2009; Hafke and van Bel, 2013).

It was previously shown that forisome responses depend on the cooling regime (Thorpe et al., 2010). Using cooling steps (slower cooling followed by a much longer period of low temperature), forisome recontraction is clearly related to the absolute temperature attributed to the temperature dependence of the SE-plasma membrane or smooth ER-$Ca^{2+}$ pump (Thorpe et al., 2010, and refs. therein). In this work, cold shocks (very rapid but brief cooling; Thorpe et al., 2010) did not reveal a distinct temperature dependence, as indicated by scattered data points (Fig. 4J).

Maximal $\Delta V_1$ ($\Delta T \geq 4$°C) is likely implemented by $Ca^{2+}$-dependent $Cl^-$ channels, as shown for other cell types (Lewis et al., 1997; Krol et al., 2004, and refs. therein). Repolarization depends on $K^+$-outward channels (Trebacz et al., 1994; Krol et al., 2003; Supplemental Fig. S2) identified at the plasma membrane of isolated SE protoplasts (Hafke et al., 2007). These channels open before the Nernst potential for $Cl^-$ is reached at $V_m$ positive to the Nernst potential for $K^+$ and cause $K^+$ efflux, which repolarizes the membrane to the equilibrium potential for $K^+$ (Trebacz et al., 1994). With $K^+$ concentrations around 100 mM in SEs (Fromm and Lautner, 2007) and an external $K^+$ concentration of 2 mM in the bathing medium used in our experiments, the Nernst potential for $K^+$ is around −100 mV, which approximates a membrane voltage of −100 to −125 mV, the range of the onset value of $\Delta V_2$ (Fig. 4C). Repolarization of $V_m$ to levels more negative than the equilibrium potential for $K^+$ must be achieved by the electrogenic $H^+$ pumps (Trebacz et al., 1994; Krol et al., 2004). Thus, the slow kinetic phase of $\Delta V_2$ of the biphasic cold response can be assumed to be dictated by the $H^+$ pump that restores the $V_m$ resting level (Fig. 4, F and G).

In the case of severe cold shocks causing pressure drops in SEs (Gould et al., 2004), repolarization is possibly delayed by down-regulation of the $H^+$ pump. In fava bean, the $H^+$ pump is inhibited by intracellular $Ca^{2+}$, with a half-inhibitory concentration of 0.3 μM (Kinoshita et al., 1995). This value matches well the cytosolic $Ca^{2+}$ elevations triggered by local cold shocks (0.1–1 μM; Plieth et al., 1999). Since intracellular $Ca^{2+}$ increases with cold shock strength (Plieth et al., 1999; Fig. 4I), the enhanced repolarization periods at higher stimulus strengths (Fig. 4, C and G) may be explained by a $Ca^{2+}$-dependent inhibition of the proton pump. In line with this idea, the suppression of a $Ca^{2+}$ influx into SEs in the presence of external $La^{3+}$ accelerates repolarization to the resting $V_m$ (Fig. 4D) as compared with the control (Fig. 4, C and G). Delayed recovery of $H^+$-ATPase activity, owing to severed supply of ATP due to pore plasmodesma unit occlusion (Furch et al., 2007), may also limit restoration of the $V_m$.

### Effects of LatA and CytD on $Ca^{2+}$ Influx and Forisome Conformation

The control of transmembrane ion fluxes by cytoskeleton organization plays a pivotal role in the transduction of external stimuli like temperature and wounding in parenchymatous cells (Mazars et al., 1997, and refs. therein). Cytoskeleton disruptors that destabilize either F-actin (Liu and Luan, 1998; Wang et al., 2004; Zhang et al., 2007) or microtubules (Thion et al., 1998) affect the action of ion channels, as demonstrated by patch clamping (Liu and Luan, 1998; Thion et al., 1998; Wang et al., 2004; Zhang et al., 2007) or $Ca^{2+}$ fluorescence imaging (Mazars et al., 1997; Wang et al., 2004).

The effects of actin filament disruptors on $Ca^{2+}$ channels or $Ca^{2+}$ gradients are discussed controversially. Patch-clamp studies (Wang et al., 2004; Zhang et al., 2007) demonstrated increased $Ca^{2+}$ fluxes in the presence of the cytoskeleton disruptors CytD or LatA. In line with this observation, Örvar et al. (2000) showed that cold-induced $Ca^{2+}$ influx in alfalfa (*Medicago sativa*) cells was prevented by the microfilament-stabilizing agent jasplakinolide and induced at 25°C by the actin filament destabilizer CytD. They proposed that CytD-induced $Ca^{2+}$ influx does not require the depolymerization of actin filaments but, instead, remodeling of the preexisting network.

In contrast, latrunculin B treatment decreased intracellular $Ca^{2+}$ in pollen tubes, evidenced by a drastically reduced tip-focused $Ca^{2+}$ gradient associated with a degradation of the actin cytoskeleton (Cárdenas et al., 2008). Wang et al. (2010) united both views by proposing that the actin-degrading agent latrunculin B induces an increase followed by a decrease of cytosolic $Ca^{2+}$ in root hairs of Arabidopsis.

We found that disruption of actin filaments by 500 nM LatA decreases the $\Delta V_1$ response to local cold shocks (Fig. 5, A and C), indicative of a lower $Ca^{2+}$ influx into SEs and, in line with this, a suppression of the $Ca^{2+}$-dependent forisome dispersion. Abolished or reduced $Ca^{2+}$ signals after LatA treatments were previously demonstrated for various animal cell types (Lange and Gartzke,

2006, and refs. therein). The addition of $La^{3+}$ does not significantly alter the inhibitory effect of LatA (Fig. 4D), suggesting that the two effectors act on the same $Ca^{2+}$ influx system located in the SE plasma membrane. Whether actin filaments also play a role in $Ca^{2+}$ release from the internal stores involved in forisome dispersion (Furch et al., 2009; Hafke et al., 2009; Thorpe et al., 2010), as proposed for animal cells (Janmey, 1998, and refs. therein; Lange and Gartzke, 2006, and refs. therein), cannot be answered as yet.

Furthermore, the SE response to actin disruption seems to be dose dependent, as 250 nM LatA showed an initial depolarization $\Delta V_1$ after cold shocks that is nearly comparable to measurements under control conditions (Fig. 5C). The actin disruptor CytD, in contrast, did not change the initial voltage transient significantly (Supplemental Fig. S1A), nor does it alter the forisome response to cold shocks (Supplemental Fig. 1, B and C). This is in agreement with the observation that LatA (Fig. 5) is 10- to 100-fold more effective in disrupting actin filaments than CytD (Spector et al., 1989). As mentioned above, CytD seems to force a rearrangement of actin filaments rather than a complete disruption (Örvar et al., 2000), which might be necessary to sever $Ca^{2+}$ channel function.

If the nature or the dose of the actin filament modulator dictates the cytoskeleton conformation and alters the electrical signals and the forisome reaction of SEs, this might have further consequences for other actin-mediated cellular responses. Microfilaments are regarded as important targets for signaling information and as transducers of signals (Drøbak et al., 2004) by binding to the plasma membrane via integrin-like proteins (Ingber, 1991; Trewavas and Malho, 1997; Knepper et al., 2011; Lü et al., 2012). As a prime candidate for actin/membrane interactions, the plant specific NETWORKED superfamily of membrane-associated actin-binding proteins was identified recently, allowing actin-membrane interactions via a novel actin-binding domain (Deeks et al., 2012). It was hypothesized that protein complexes designated as "transducons" are formed at the attachment sites (Trewavas and Malho, 1997), which consist of an aggregate of receptors, $Ca^{2+}$ channels, bound calmodulin, protein kinases and phosphatases, and $Ca^{2+}$-ATPases (Trewavas and Malho, 1997).

## CONCLUSION

(1) It is a major issue if cold shocks induce $Ca^{2+}$ influx via mechanical tension imposed by structural changes in the plasma membrane or via mechanical forces on cytoskeleton components attached to $Ca^{2+}$ channels. Given the effects of cytoskeleton disruptors, the second scenario seems to be the more likely one at this stage.

(2) Reactivity to cold shocks may reflect the ability of the SEs to react to mechanical perturbations of any origin. Thus, $Ca^{2+}$-permeable channels in a still unidentified interaction with cytoskeleton elements may also react to the frequent pressure changes in sieve tubes and, hence, play a major role in the regulation of pressure gradients.

(3) The extent to which the propagation of cold-induced electrical potential waves (Fromm and Lautner, 2007; Hafke and van Bel, 2013) has an impact on the cytoskeleton of remote SEs remains to be investigated.

(4) SEs may be ideal systems to study the interaction between the plasma membrane and cytoskeleton in signaling cascades. The interpretation of such experiments may be far easier than in parenchyma cells, with their much higher degree of structural complexity.

## MATERIALS AND METHODS

### Plants

Fava bean (*Vicia faba* 'Witkiem major') plants (Nunhems Zaden) were grown at 25°C and 60% to 70% relative humidity in a greenhouse under a 14/10-h light/dark regime with supplementary lighting (SONT Agro 400-W lamps; Philips) giving 200 to 250 $\mu$mol $m^{-2}$ $s^{-1}$ photosynthetically active radiation at the plant apex. Plants were used in the vegetative phase, 17 to 21 d after germination.

### Preparation of Intact Plant Tissues for Microinjection and Electrophysiology

For in vivo observation of sieve tubes, cortical cell layers were removed from the abaxial side of the main vein of the youngest mature leaflet to expose the phloem by manual paradermal slicing with a fresh razor blade, according to Knoblauch and van Bel (1998). The leaflet, which was still attached to the plant, was mounted on a microscope slide on the microscope stage using double-sided adhesive tape, the abaxial side uppermost (i.e. the leaf was upside down). The exposed tissue was covered with a bathing medium (BM) containing 2 mM KCl, 1 mM $CaCl_2$, 1 mM $MgCl_2$, 50 mM mannitol, and 2.5 mM MES/NaOH at pH 5.7 (Hafke et al., 2005) for at least 60 min before any further treatment was conducted.

### Microinjection of Alexa Fluor 546 Phalloidin and Reactive Alexa Fluor 546 Succinimidyl Ester

#### *Alexa Fluor 546 Phalloidin*

Injection capillaries were pulled from borosilicate glass with an internal filament and an o.d. of 1 mm (GC100F-10; Harvard Apparatus) on an L/M-3P-A two-stage puller (List Medical) to give an outer tip diameter of approximately 1 $\mu$m. Injection capillaries were back filled with a small volume of Alexa Fluor 546 phalloidin (Invitrogen; 6.6 $\mu$M in methanol), a high-affinity probe for F-actin, filled up with silicon oil, and connected with a pressure device (Cell Tram Oil microinjector; Eppendorf).

After maneuvering the microelectrodes toward the phloem tissue by means of a micromanipulator (LN SM-1; Luigs and Neumann), SEs were impaled. After successful impalement, gentle pressure was exerted on the injection capillary to expel a small volume of fl-phal. Microinjection was monitored with a Leica DM-LB fluorescence microscope (HCX APO L40X/0.80 W U-V-I water-immersion objective, filter block N2.1; Leica Microsystems) as described before (Hafke et al., 2005), and the fluorescent tissues were scanned using CLSM after the completion of staining.

#### *Alexa Fluor 546 Succinimidyl Ester*

Succinimidyl esters provide an efficient and convenient way to selectively link the Alexa Fluor dyes to primary amines (R-$NH_2$) located on peptides, proteins, or amine-modified nucleic acids (data sheet from Invitrogen/Molecular Probes).

Alexa Fluor 546 succinimidyl ester (Invitrogen) was dissolved in anhydrous DMSO (final concentration of 5 mM), and aliquots of the stock solution were diluted with BM to give a final concentration of 5 $\mu$M in DMSO/BM to be used for microinjection into SEs. The hydrolyzed nonreactive derivative of Alexa Fluor 546 succinimidyl ester (compare with www.lumiprobe.com; Protocol: NHS Ester Labeling of Amino-Biomolecules) was prepared by adding 50 mM

Tris buffer to a stock solution of the reactive ester to give a final concentration of 5 $\mu$M. After incubation at 4°C for 12 h in the dark, the resultant hydrolysate was microinjected into SEs as described above.

## CLSM

Fluorochrome distribution was visualized by a Leica TCS 4D CLSM device (Leica Microsystems) equipped with a 75-mW argon/krypton laser as described before (Knoblauch and van Bel, 1998; Furch et al., 2009). Tissues were observed with a water-immersion objective (HCX APO L40x /0.80 W U-V-I; Leica Microsytems) in the dipping mode. Alexa Fluor 546 derivatives were excited by the 564-nm line, and fluorescence was observed at 590 nm. Images were processed using Adobe PhotoShop and Corel Photo Paint to optimize brightness, contrast, and color.

## Forisome Observation

Forisome responses under control conditions and in the presence of cytoskeleton disruptors subsequent to cold shock were observed using light microscopy as described previously (Thorpe et al., 2010). Cold shocks were exerted locally on SEs pretreated with BM or cytoskeleton-disrupting agents.

## Immunocytochemistry and Transmission Electron Microscopy

About 40-mm-long internodal segments of fava bean stems were longitudinally halved. SEs in the segments were allowed to recover for 2 h from mechanical injury before being submerged in a medium containing 10 mM KCl, 10 mM $CaCl_2$, and 5 mM NaCl in double-distilled water (Ehlers et al., 2000). During 4.5 h of chemical fixation at room temperature in a solution of 4% (w/v) paraformaldehyde and 0.75% (v/v) glutardialdehyde in 0.1 M sodium phosphate buffer plus 1% (w/v) tannic acid (pH 7.2), the fixative was replaced every 1.5 h. After washing three times in 0.1 M sodium phosphate buffer and three times in distilled water on ice, en-bloc staining was performed with 0.5% (w/v) aqueous uranyl acetate for 30 min on ice. Segments were dehydrated in a graded ethanol series and transferred into unicryl resin (British BioCell International). Immediately before embedding in gelatin capsules, the cut surface was removed from either end of the internodal segments, and the segments were cut into smaller samples. Polymerization was performed at 52°C for 2 d.

Longitudinal, ultrathin sections were cut from the median zones of the samples with a diamond knife on a Reichert Om U2 ultramicrotome (Leica) and were collected on Formvar-coated single-slot gold grids. For indirect immunolocalization, all sections were blocked with 5% (w/v) bovine serum albumin (BSA) in 0.1 M phosphate-buffered saline (PBS) buffer (pH 7.2) for 1.5 h. Thereafter, some grids were incubated for 1.5 h with mouse anti-actin (clone C4, MAB 1501; Millipore) diluted 1:100 (v/v) in 0.1 M PBS with 0.5% (w/v) BSA. These grids were washed nonstringently once in 0.1 M PBS containing 0.01% (v/v) Tween 20 (Sigma-Aldrich) and two more times in 0.1 M PBS for 10 min each. Other grids with serial sections were incubated for 1.5 h with the primary anti-actin antibody diluted 1:200 (v/v) in 0.1 M PBS with 0.5% (w/v) BSA and washed stringently three times in 0.1 M PBS containing 0.01% (v/v) Tween 20 for 10 min each. Controls were incubated in 0.1 M PBS with 0.5% (w/v) BSA only and washed stringently or nonstringently. All sections were then treated with 5-nm gold-labeled goat anti-mouse IgG (whole molecule; G7527; Sigma-Aldrich) diluted 1:50 (v/v) in 0.1 M PBS with 0.5% (w/v) BSA for 1 h and washed again following the procedures mentioned above. Finally, antibodies on the sections were fixed with 3% (v/v) glutardialdehyde for 10 min, and the grids were rinsed with demineralized water before they were poststained with Reynolds' lead citrate (Reynolds, 1963) and 2% (w/v) aqueous uranyl acetate. All treatments were performed at room temperature.

Ultrathin sections were examined at 120 kV in a LEO EM 912 Ω AB transmission electron microscope (Zeiss). Digital electron micrographs were taken with an integrated slow-scan CCD camera (Proscan), and image processing was performed with Corel PHOTO PAINT 10 and Corel DRAW 10.

## Electrophysiology

$V_m$ measurements of SEs in intact fava bean plants were described in detail previously (Hafke et al., 2005). Microelectrodes with a tip diameter of 0.5 to 1 $\mu$m were pulled on a vertical electrode puller (GETRA) from aluminosilicate microcapillaries having an o.d. of 1 mm and an internal filament (SM100F-10; Harvard Apparatus). The glass capillaries were back filled with 500 mM KCl and clamped in an Ag/AgCl pellet electrode holder (World Precision Instruments). The microelectrode was connected to the probe of an amplifier (DUO 773 high-input impedance differential electrometer; World Precision Instruments). The Ag/AgCl reference electrode was connected to the leaf by a 2% (w/v) agar bridge made up with 500 mM KCl.

After submersion of the exposed phloem tissue in BM for 1 h (see "Preparation of the Intact Plant Tissues" above), SEs were impaled with the microelectrode under continuous microscopic surveillance using an LN SM-1 micromanipulator (Luigs and Neumann). After stabilization of the SE resting potential, a cold shock (very rapid pulse, but brief cooling) was applied to the same SE assayed by a pipette filled with tempered BM while recording changes in SE-$V_m$ by a microelectrode (Hafke et al., 2005). The $\Delta$T (difference between the initial temperature and the lowest temperature at the end of the drop) was recorded by a thermocouple as described before (Thorpe et al., 2010). Cytoskeleton disruptors were prepared as stock solutions dissolved in DMSO and diluted in BM to give the following final working concentrations (with final DMSO contents of the working solution in parentheses): 40 $\mu$M CytD (0.1% [v/v] DMSO), 0.25 $\mu$M (0.005% [v/v] DMSO), and 0.5 $\mu$M LatA (0.01% [v/v] DMSO). $LaCl_3$, a $Ca^{2+}$ channel blocker, was prepared as a stock solution of 100 mM dissolved in water and diluted to a final concentration of 1 mM in BM. CytD and LatA were purchased from Invitrogen, and $LaCl_3$ was purchased from Sigma-Aldrich.

Subsequent to the incubation of prepared phloem tissue with $La^{3+}$, the respective cytoskeleton disruptors, or BM (control) for 1.5 to 2 h, the phloem surface was washed with BM before electrical responses were triggered by local cold shocks. Phloem tissue preparations exposing free-lying sieve tubes (no cell layers above) ensured binding of the drugs to the $Ca^{2+}$ channels of the SE plasma membrane or to the SE cytoskeleton as well as the comparability of the measurements. Electrophysiological data were processed using SigmaPlot 11 software (Systat Software).

## Supplemental Data

The following materials are available in the online version of this article.

**Supplemental Figure S1.** Effect of cytochalasin D on electrical signals and forisome behavior in response to cold shocks.

**Supplemental Figure S2.** Effect of the $K^+$-channel inhibitor tetraethylammonium chloride (TEA-Cl) on electrical signals in sieve elements.

Received February 10, 2013; accepted April 26, 2013; published April 26, 2013.

## LITERATURE CITED

**Aki T, Shigyo M, Nakano R, Yoneyama T, Yanagisawa S** (2008) Nano scale proteomics revealed the presence of regulatory proteins including three FT-Like proteins in phloem and xylem saps from rice. Plant Cell Physiol **49:** 767–790

**Barnes A, Bale J, Constantinidou C, Ashton P, Jones A, Pritchard J** (2004) Determining protein identity from sieve element sap in *Ricinus communis* L. by quadrupole time of flight (Q-TOF) mass spectrometry. J Exp Bot **55:** 1473–1481

**Blackman LM, Boevink P, Cruz SS, Palukaitis P, Oparka KJ** (1998) The movement protein of cucumber mosaic virus traffics into sieve elements in minor veins of *Nicotiana clevelandii*. Plant Cell **10:** 525–538

**Boevink P, Oparka KJ, Santa Cruz S, Martin B, Betteridge A, Hawes C** (1998) Stacks on tracks: the plant Golgi apparatus traffics on an actin/ER network. Plant J **15:** 441–447

**Cárdenas L, Lovy-Wheeler A, Kunkel JG, Hepler PK** (2008) Pollen tube growth oscillations and intracellular calcium levels are reversibly modulated by actin polymerization. Plant Physiol **146:** 1611–1621

**Carpaneto A, Ivashikina N, Levchenko V, Krol E, Jeworutzki E, Zhu J-K, Hedrich R** (2007) Cold transiently activates calcium-permeable channels in Arabidopsis mesophyll cells. Plant Physiol **143:** 487–494

**Chaffey N, Barlow P** (2002) Myosin, microtubules, and microfilaments: cooperation between cytoskeletal components during cambial cell division and secondary vascular differentiation in trees. Planta **214:** 526–536

**Chen J, Doyle C, Qi X, Zheng H** (2012) The endoplasmic reticulum: a social network in plant cells. J Integr Plant Biol **54:** 840–850

**Chérel I** (2004) Regulation of $K^+$ channel activities in plants: from physiological to molecular aspects. J Exp Bot **55:** 337–351

**Cooper JA** (1987) Effects of cytochalasin and phalloidin on actin. J Cell Biol **105:** 1473–1478

**Davies E, Stankovic B** (2006) Electrical signals, the cytoskeleton and gene expression: a hypothesis on the coherence of the cellular responses to environmental insult. *In* F Baluška, S Mancuso, D Volkmann, eds, Communication in Plants. Springer-Verlag, Berlin, pp 309–320

**Deeks MJ, Calcutt JR, Ingle EKS, Hawkins TJ, Chapman S, Richardson AC, Mentlak DA, Dixon MR, Cartwright F, Smertenko AP, et al** (2012) A superfamily of actin-binding proteins at the actin-membrane nexus of higher plants. Curr Biol **22:** 1595–1600

**Ding JP, Pickard BG** (1993) Modulation of mechanosensitive calcium-selective cation channels by temperature. Plant J **3:** 713–720

**Drøbak BK, Franklin-Tong VE, Staiger CJ** (2004) The role of the actin cytoskeleton in plant cell signaling. New Phytol **163:** 13–30

**Ehlers K, Knoblauch M, van Bel AJE** (2000) Ultrastructural features of well-preserved and injured sieve elements: minute clamps keep the phloem transport conduits free for mass flow. Protoplasma **214:** 80–92

**Evert R** (1990) Dicotyledons. *In* H-D Behnke, RD Sjolund, eds, Sieve-Elements: Comparative Structure, Induction and Development. Springer-Verlag, Berlin, pp 103–137

**Fisher DB, Wu Y, Ku MSB** (1992) Turnover of soluble proteins in the wheat sieve tube. Plant Physiol **100:** 1433–1441

**Fromm J, Lautner S** (2007) Electrical signals and their physiological significance in plants. Plant Cell Environ **30:** 249–257

**Furch ACU, Hafke JB, Schulz A, van Bel AJE** (2007) $Ca^{2+}$-mediated remote control of reversible sieve tube occlusion in *Vicia faba*. J Exp Bot **58:** 2827–2838

**Furch ACU, van Bel AJE, Fricker MD, Felle HH, Fuchs M, Hafke JB** (2009) Sieve element $Ca^{2+}$ channels as relay stations between remote stimuli and sieve tube occlusion in *Vicia faba*. Plant Cell **21:** 2118–2132

**Giavalisco P, Kapitza K, Kolasa A, Buhtz A, Kehr J** (2006) Towards the proteome of *Brassica napus* phloem sap. Proteomics **6:** 896–909

**Gould N, Thorpe MR, Minchin PEH** (2004) Direct measurements of sieve element hydrostatic pressure reveal strong regulation of sieve element hydrostatic pressure after pathway blockage. Funct Plant Biol **31:** 987–993

**Hafke JB, Furch ACU, Fricker MD, van Bel AJE** (2009) Forisome dispersion in *Vicia faba* is triggered by $Ca^{2+}$ hotspots created by concerted action of diverse $Ca^{2+}$ channels in sieve elements. Plant Signal Behav **4:** 968–972

**Hafke JB, Furch ACU, Reitz MU, van Bel AJE** (2007) Functional sieve element protoplasts. Plant Physiol **145:** 703–711

**Hafke JB, van Amerongen J-K, Kelling F, Furch ACU, Gaupels F, van Bel AJE** (2005) Thermodynamic battle for photosynthate acquisition between sieve tubes and adjoining parenchyma in transport phloem. Plant Physiol **138:** 1527–1537

**Hafke JB, van Bel AJE** (2013) Cellular basis of electrical potential waves along the phloem and impact of coincident $Ca^{2+}$ fluxes. *In* GA Thompson, AJE van Bel, eds, Phloem: Molecular Cell Biology, Systemic Communication, Biotic Interactions. Wiley-Blackwell, Hoboken, NJ, pp 122–140

**Hayakawa K, Tatsumi H, Sokabe M** (2008) Actin stress fibers transmit and focus force to activate mechanosensitive channels. J Cell Sci **121:** 496–503

**Hepler PK, Palevitz BA, Lancelle SA, McCauley MM, Lichtscheidl L** (1990) Cortical endoplasmic reticulum in plants. J Cell Sci **96:** 355–373

**Heslop-Harrison J, Heslop-Harrison Y** (1997) Intracellular motility and the evolution of the actin cytoskeleton during development of the male gametophyte of wheat (*Triticum aestivum* L.). Philos Trans R Soc Lond **352:** 1985–1993

**Hille B** (1992) Mechanisms of block. *In* B Hille, ed, Ionic Channels of Excitable Membranes, Ed 2. Sinauer Associates, Sunderland, MA, pp 390–423

**Hwang J-U, Suh S, Yi H, Kim J, Lee Y** (1997) Actin filaments modulate both stomatal opening and inward $K^+$-channel activities in guard cells of *Vicia faba* L. Plant Physiol **115:** 335–342

**Ingber DE** (1991) Integrins as mechanochemical transducers. Curr Opin Cell Biol **3:** 841–848

**Janmey PA** (1998) The cytoskeleton and cell signaling: component localization and mechanical coupling. Physiol Rev **78:** 763–781

**Kinoshita T, Nishimura M, Shimazaki K** (1995) Cytosolic concentration of $Ca^{2+}$ regulates the plasma membrane $H^+$-ATPase in guard cells of fava bean. Plant Cell **7:** 1333–1342

**Knepper C, Savory EA, Day B** (2011) Arabidopsis NDR1 is an integrin-like protein with a role in fluid loss and plasma membrane-cell wall adhesion. Plant Physiol **156:** 286–300

**Knight H, Trewavas AJ, Knight MR** (1996) Cold calcium signaling in *Arabidopsis* involves two cellular pools and a change in calcium signature after acclimation. Plant Cell **8:** 489–503

**Knoblauch M, Peters WS, Ehlers K, van Bel AJE** (2001) Reversible calcium-regulated stopcocks in legume sieve tubes. Plant Cell **13:** 1221–1230

**Knoblauch M, van Bel AJE** (1998) Sieve tubes in action. Plant Cell **10:** 35–50

**Krol E, Dziubinska H, Trebacz K** (2003) Low-temperature induced transmembrane potential changes in the liverwort *Conocephalum conicum*. Plant Cell Physiol **44:** 527–533

**Krol E, Dziubińska H, Trebacz K** (2004) Low-temperature-induced transmembrane potential changes in mesophyll cells of *Arabidopsis thaliana*, *Helianthus annuus* and *Vicia faba*. Physiol Plant **120:** 265–270

**Krol E, Trebacz K** (1999) Calcium-dependent voltage transients evoked by illumination in the liverwort *Conocephalum conicum*. Plant Cell Physiol **40:** 17–24

**Kulikova AL, Puryaseva AP** (2002) Actin in pumpkin phloem exudate. Russ J Plant Physiol **49:** 54–60

**Lange K, Gartzke J** (2006) F-actin-based Ca signaling: a critical comparison with the current concept of Ca signaling. J Cell Physiol **209:** 270–287

**Leineweber K, Schulz A, Thompson GA** (2000) Dynamic transitions in the translocated phloem filament protein. Aust J Plant Physiol **27:** 733–741

**Lengsfeld AM, Löw I, Wieland T, Dancker P, Hasselbach W** (1974) Interaction of phalloidin with actin. Proc Natl Acad Sci USA **71:** 2803–2807

**Lewis BD, Karlin-Neumann G, Davis RW, Spalding EP** (1997) $Ca^{2+}$-activated anion channels and membrane depolarizations induced by blue light and cold in Arabidopsis seedlings. Plant Physiol **114:** 1327–1334

**Lewis BD, Spalding EP** (1998) Nonselective block by $La^{3+}$ of Arabidopsis ion channels involved in signal transduction. J Membr Biol **162:** 81–90

**Liu K, Luan S** (1998) Voltage-dependent $K^+$ channels as targets of osmosensing in guard cells. Plant Cell **10:** 1957–1970

**Lloyd C** (1988) Actin in plants. J Cell Sci **90:** 185–188

**Lü B, Wang J, Zhang Y, Wang H, Liang J, Zhang J** (2012) AT14A mediates the cell wall-plasma membrane-cytoskeleton continuum in *Arabidopsis thaliana* cells. J Exp Bot **63:** 4061–4069

**Lucas WJ, Yoo B-C, Kragler F** (2001) RNA as a long-distance information macromolecule in plants. Nat Rev Mol Cell Biol **2:** 849–857

**Mazars C, Thion L, Thuleau P, Graziana A, Knight MR, Moreau M, Ranjeva R** (1997) Organization of cytoskeleton controls the changes in cytosolic calcium of cold-shocked *Nicotiana plumbaginifolia* protoplasts. Cell Calcium **22:** 413–420

**Minorsky PV, Spanswick RM** (1989) Electrophysiological evidence for a role for calcium in temperature sensing by roots of cucumber seedlings. Plant Cell Environ **12:** 137–143

**Oparka KJ** (2004) Getting the message across: how do plant cells exchange macromolecular complexes? Trends Plant Sci **9:** 33–41

**Örvar BL, Sangwan V, Omann F, Dhindsa RS** (2000) Early steps in cold sensing by plant cells: the role of actin cytoskeleton and membrane fluidity. Plant J **23:** 785–794

**Parthasarathy MV, Pesacreta TC** (1980) Microfilaments in plant vascular cells. Can J Bot **58:** 807–815

**Plieth C, Hansen U-P, Knight H, Knight MR** (1999) Temperature sensing by plants: the primary characteristics of signal perception and calcium response. Plant J **18:** 491–497

**Reynolds ES** (1963) The use of lead citrate at high pH as an electron-opaque stain in electron microscopy. J Cell Biol **17:** 208–212

**Sangwan V, Foulds I, Singh J, Dhindsa RS** (2001) Cold-activation of *Brassica napus BN115* promoter is mediated by structural changes in membranes and cytoskeleton, and requires $Ca^{2+}$ influx. Plant J **27:** 1–12

**Schobert C, Baker L, Szederényi J, Großmann P, Komor E, Hayashi H, Chino M, Lucas WJ** (1998) Identification of immunologically related proteins in sieve-tube exudates collected from monocotyledonous and dicotyledonous plants. Planta **206:** 245–252

**Schobert C, Gottschalk M, Kovar DR, Staiger CJ, Yoo B-C, Lucas WJ** (2000) Characterization of *Ricinus communis* phloem profilin, RcPRO1. Plant Mol Biol **42:** 719–730

**Spector I, Shochet NR, Blasberger D, Kashman Y** (1989) Latrunculins: novel marine macrolides that disrupt microfilament organization and affect cell growth. I. Comparison with cytochalasin D. Cell Motil Cytoskeleton **13:** 127–144

**Thion L, Mazars C, Nacry P, Bouchez D, Moreau M, Ranjeva R, Thuleau P** (1998) Plasma membrane depolarization-activated calcium channels, stimulated by microtubule-depolymerizing drugs in wild-type Arabidopsis thaliana protoplasts, display constitutively large activities and a longer half-life in ton 2 mutant cells affected in the organization of cortical microtubules. Plant J **13:** 603–610

**Thorpe MR, Furch ACU, Minchin PEH, Föller J, Van Bel AJE, Hafke JB** (2010) Rapid cooling triggers forisome dispersion just before phloem transport stops. Plant Cell Environ **33:** 259–271

**Thorsch J, Esau K** (1981) Nuclear degeneration and the association of endoplasmic reticulum with the nuclear envelope and microtubules in maturing sieve elements of *Gossypium hirsutum*. J Ultrastruct Res **74:** 195–204

**Thuleau P, Schroeder JI, Ranjeva R** (1998) Recent advances in the regulation of plant calcium channels: evidence for regulation by G-proteins, the cytoskeleton and second messengers. Curr Opin Plant Biol **1:** 424–427

**Tiwari SC, Polito VS** (1988) Spatial and temporal organization of actin during hydration, activation, and germination of pollen in *Pyrus communis*: a population study. Protoplasma **147:** 5–15

**Trebacz K, Simonis W, Schönknecht G** (1994) Cytoplasmic $Ca^{2+}$, $K^+$, $Cl^-$ and $NO_3^-$ activities in the liverwort *Conocephalum conicum* L. at rest and during action potentials. Plant Physiol **106:** 1073–1084

**Trewavas AJ, Malho R** (1997) Signal perception and transduction: the origin of the phenotype. Plant Cell **9:** 1181–1195

**Ueda H, Yokota E, Kutsuna N, Shimada T, Tamura K, Shimmen T, Hasezawa S, Dolja VV, Hara-Nishimura I** (2010) Myosin-dependent endoplasmic reticulum motility and F-actin organization in plant cells. Proc Natl Acad Sci USA **107:** 6894–6899

**van Bel AJE, Knoblauch M, Furch ACU, Hafke JB** (2011) (Questions)($^n$) on phloem biology. 1. Electropotential waves, $Ca^{2+}$ fluxes and cellular cascades along the propagation pathway. Plant Sci **181:** 210–218

**Walz C, Giavalisco P, Schad M, Juenger M, Klose J, Kehr J** (2004) Proteomics of curcurbit phloem exudate reveals a network of defence proteins. Phytochemistry **65:** 1795–1804

**Wang Y, Zhu Y, Ling Y, Liu P, Baluska F, Samaj J, Lin J, Wang Q** (2010) Disruption of actin filaments induces mitochondrial $Ca^{2+}$ release to the cytoplasm and $[Ca^{2+}]_c$ changes in *Arabidopsis* root hairs. Plant Biol **10:** 1–13

**Wang YF, Fan L-M, Zhang W-Z, Zhang W, Wu W-H** (2004) $Ca^{2+}$-permeable channels in the plasma membrane of Arabidopsis pollen are regulated by actin microfilaments. Plant Physiol **136:** 3892–3904

**White PJ** (2009) Depolarization-activated calcium channels shape the calcium signatures induced by low-temperature stress. New Phytol **183:** 6–8

**Will T, van Bel AJE** (2006) Physical and chemical interactions between aphids and plants. J Exp Bot **57:** 729–737

**Yokota E, Ueda H, Hashimoto K, Orii H, Shimada T, Hara-Nishimura I, Shimmen T** (2011) Myosin XI-dependent formation of tubular structures from endoplasmic reticulum isolated from tobacco cultured BY-2 cells. Plant Physiol **156:** 129–143

**Zhang W, Fan LM, Wu WH** (2007) Osmo-sensitive and stretch-activated calcium-permeable channels in *Vicia faba* guard cells are regulated by actin dynamics. Plant Physiol **143:** 1140–1151